

**TITLE: Post-Mortem Findings in Italian Patients with Covid-19 – a Descriptive Full Autopsy Study of cases with and without co-morbidities.**

**AUTHORS:** Laura Falasca<sup>1\*</sup>, Roberta Nardacci<sup>1\*#</sup>, Daniele Colombo<sup>1</sup>, Eleonora Lalle<sup>1</sup>, Antonino Di Caro<sup>1</sup>, Emanuele Nicastri<sup>1</sup>, Andrea Antinori<sup>1</sup>, Nicola Petrosillo<sup>1</sup>, Luisa Marchioni<sup>1</sup>, Gianluigi Biava<sup>1</sup>, Gianpiero D'Offizi<sup>1</sup>, Fabrizio Palmieri<sup>1</sup>, Delia Goletti<sup>1</sup>, Alimuddin Zumla<sup>2\*</sup>, Giuseppe Ippolito<sup>1\*</sup>, Mauro Piacentini<sup>1,3\*</sup> and Franca Del Nonno<sup>1\*</sup> - on behalf of COVID 19 INMI Study Group.

\*Contributed equally

**INSTITUTIONAL AFFILIATIONS:**

- 1) National Institute for Infectious Diseases Lazzaro Spallanzani-IRCCS, Rome, Italy.
- 2) Department of Infection, Division of Infection and Immunity, University College London and NIHR Biomedical Research Centre, UCL Hospitals NHS Foundation Trust, London, United Kingdom.
- 3) Laboratory of Cellular and Developmental Biology, Department of Biology of the University of Rome, "Tor Vergata", Rome, Italy.

**KEYPOINTS: (40 words):**

Autopsy findings in patients with COVID-19 showed deaths were due to cardiorespiratory failure, predominantly caused by acute lung injury, microvascular damage and thrombosis. COVID-19 causes multisystem disease and significant pathology in most organs in patients with and without co-morbidities.

**RUNNING TITLE: Autopsy findings in COVID-19**

**#CORRESPONDING AUTHOR:** Dr. Roberta Nardacci: INMI-I.R.C.C.S. "L. Spallanzani"Via Portuense, 292 –00149 Roma, Italia. Telephone: 06-55170429 Email: [roberta.nardacci@inmi.it](mailto:roberta.nardacci@inmi.it)

## **ABSTRACT**

### **Background.**

Descriptions of the pathological features of CoronaVirus Disease-2019 (COVID-19) caused by the novel zoonotic pathogen Severe Acute Respiratory Syndrome Coronavirus-2 (SARS-CoV-2) emanate from tissue biopsies, case reports and small post-mortem studies restricted to the lung and specific organs. Whole body autopsy studies of COVID-19 patients have been sparse. To further define the pathological manifestations across all body organs in individuals with and without co-morbidities, we performed an autopsy study of Italian patients who died of COVID-19.

### **Methods.**

We performed autopsies on 22 patients with COVID-19 (18 with co-morbidities and 4 without co-morbidities) who died at the National Institute for Infectious Diseases Lazzaro Spallanzani-IRCCS Hospital, Rome, Italy. Tissues from the lung, heart, liver, kidney, spleen and bone marrow (but not the brain) were examined. Only lung tissues were subject to transmission electron microscopy.

### **Results.**

COVID-19 causes multisystem pathology. Pulmonary and cardiovascular involvement are dominant pathological features. Extra-pulmonary manifestations include hepatic, kidney, splenic and bone marrow involvement, and microvascular injury and thrombosis were also detected. These findings were similar in patients with or without pre-existing medical co-morbidities.

**Conclusions.** SARS-CoV-2 infection causes multisystem disease and significant pathology in most organs in patients with and without co-morbidities.

**Keywords.** Autopsy, COVID-19, co-morbidities, SARS-CoV-2, pathology

## **INTRODUCTION**

The first human cases of COronaVirus Disease-2019 (COVID-19), caused by the novel zoonotic pathogen Severe Acute Respiratory Syndrome Coronavirus-2 (SARS-CoV-2), were first reported at the end of December 2019 from Wuhan, China. On March 12th, 2020, the WHO declared COVID-19 a global pandemic since it rapidly spread worldwide [1]. In Italy the first confirmed cases of COVID19 were reported on January 31<sup>st</sup>, were two tourists from Wuhan, China. As of August 19 2020, globally there have been 21,300,000 COVID-19 cases with 760,000 deaths reported to the WHO of which Italy has reported 250,000 COVID-19 cases with 35,000 deaths [1].

Clinical and epidemiological studies have established that COVID-19 presents as a spectrum of clinical manifestations from asymptomatic, to mild illness (up to 80% of patients) moderate (15%) to severe illness (5% patients). Increased mortality rates have been observed the elderly (>70 years of age) and those with co-morbidities [2,3]. Reports from individual or small autopsy case studies [4-6] or limited post-mortem studies [7-9] show that SARS-CoV-2, like SARS-CoV-1 was in 2003, is a multi-system disease predominantly affects the respiratory and cardiovascular system. SARS-CoV-2 has been detected in a range of clinical samples such as bronchoalveolar lavage fluid, sputum, feces, and blood indicating widespread dissemination [10]. Performing whole body autopsies in patients who die of COVID-19 remains challenging due to infection control regulations and other logistical reasons [11,12]. There is a need for more detailed and larger autopsy case series studies to further define the pathological manifestations of COVID-19 [13] and determine the full extent of organ involvement. We performed whole body post-mortem examinations of twenty-two Italian patients who died of COVID-19, four of whom had no co-morbidities.

## **METHODS**

### **Study site and Ethical approval:**

Autopsies were performed at the National Institute for Infectious Diseases Lazzaro Spallanzani-IRCCS Hospital, Rome, Italy. The study was approved by the local ethics committee (Ethics Committee approval number 9/2020).

### **Study cohort and clinical information:**

Patient demographic and clinical information was extracted from case records of 22 consecutive patients with COVID-19 who died and were autopsied.

### **Autopsy Procedures:**

Autopsies were performed using the specific guidance for post-mortem and collection and submission of specimens and biosafety practices [11] to reduce the risk of transmission of infectious pathogens during, and after, post-mortem examination. Since SARS-CoV-2 is classified as a BSL3 organisms, specific operating procedures for BSL3 pathogens were also followed. Autopsies were performed in a specific COVID-19 designated autopsy room with airflow control and airborne infection control procedures including use of appropriated PPE (i.e. NIOSH-certified disposable N-95 respirator).

### **SARS-CoV-2 RT-PCR on samples:**

SARS-CoV-2 qualitative reverse-transcriptase–polymerase-chain-reaction (RT-PCR) testing for SARS-CoV-2-infection was performed on the following samples: ocular, nasopharyngeal, oropharyngeal, lung and rectal swabs.

### **Tissues sampled and histological stains**

Since infection control regulations do not allow use of the bone saw, the brain was not examined. Tissues from the lung, heart, liver, kidney, spleen and bone marrow were placed in formalin at room temperature for 72 hours before macroscopic analysis and processing for histological examination. Tissue samples were processed using hematoxylin and eosin staining (H&E), Masson's trichrome stain, Perls' stain, reticulin stain, periodic acid-Schiff reaction (PAS) and diastase-PAS, Giemsa and/or Grocott methenamine silver stains were performed where necessary.

### **Immunohistochemistry**

Deparaffinized and rehydrated sections were used for immunohistochemistry. Organ sections were immersed in 10 mM sodium citrate, pH 6.0, and microwaved for antigen retrieval and stained on BenchMark ULTRA system fully automated instrument (Roche) with an antibody directed against CD3 (Ventana, 2GV6) CD4 (Ventana, SP35), CD8 (Ventana SP57), CD15 (Ventana MMA) CD26 (Abcam, ab28340), CD183 (BD Pharmigen, 1C6/CXCR3), CD61 (Leica, ZfZ), CD20 (Ventana, LZ6), CD68 Ventana (KP-1).

### **Transmission electron microscopy**

We only looked for evidence of SARS-CoV-2 in lung samples. Non-lung samples were not subject to TEM. Lung tissues were fixed with 2.5% glutaraldehyde in 0.1M cacodylate buffer, for 4h at 4 °C. Fixation was performed with 1% OsO<sub>4</sub>. Samples were then dehydrated in graded ethanol and

embedded in Epon resin, as previously described [14, 15]. Ultrathin sections were stained with 2% uranyl acetate and examined under a transmission electron microscope [JEOL JEM 2100 Plus (Japan Electron Optics Laboratory Co. Ltd. Tokyo, Japan).] Images were captured digitally with a digital camera TVIPS (Tietz Video and Image Processing Systems GmbH. Gauting, Germany).

## **RESULTS**

### **Patient demographics and clinical characteristics:**

**Tables 1 and 2** depict the demographic and clinical characteristics of 22 COVID-19 patients on whom post-mortem examinations were performed. 18/22 had other medical co-morbidities (**designated Group 1**). Four of them were healthy prior to hospital admission and had no known medical co-morbidities or any cause of immunosuppression (**designated Group 2**),

### **Autopsy and microscopic examination**

#### **Lung findings:**

##### *Macroscopic findings:*

Lungs from all patients were increased in volume, firm, edematous, and congested with diffuse pleural thickening and pleural effusion. Cut surface showed consolidation of lobes and red congested areas, with thickening of the interstitial septa and pulmonary edema (**Figure 1,A1**). Sub-segmental pulmonary embolism was seen in five cases.

##### *Microscopic findings:*

A range of common lung findings were seen on Light microscopy. Parenchymal multifocal damage with intra-alveolar exudative and proliferative inflammation (**Figure 1,A2**), with fibrin, hyaline membranes (**Figure 1,A3**) consistent with a diagnosis of diffuse alveolar damage (DAD) (**Table 3**). Organizing pneumonia with fibrosis and type II pneumocyte hyperplasia, amphophilic cytoplasm, large nuclei and prominent nucleoli, were indicative of cytopathic virus-induced changes (**Figure 1,A3,A4**). Fibroblastic foci consisting of loose organizing connective tissue reflective of alveolar duct fibrosis were seen (Fibrotic phase) (**Figure 1,B1**). Other findings included: Pleural fibrosis (**Figure 1,B4**), vascular injury with thrombi (**Figure 1,B2**) and vasculitis (**Figure 1,B3**). A main feature was the presence of numerous inflammatory cells consisting of granulocytes (CD15 positive) (**Figure 2, A1,A2**), macrophages (CD68+) (**Figure 2, A3,A4**), T-lymphocytes (CD3+) infiltrating into alveolar septa and clustering around capillary vessels, (**Figure 2, B1**). Immunohistochemistry showed presence of both CD4+ and CD8+ T lymphocytes (**Figure 2, B2,B3**).

Of note, lymphocytes were CD20-negative indicating an absence of infiltrating B-lymphocytes. Thrombi were present and immunohistochemistry showed presence of platelet aggregates and megakaryocytes within thrombi (**Figure 2, B4**).

*Immunohistochemistry findings:*

T-cell activation is modulated by DPP-4 [16] and thus the expression of CD26/DPP4 and CXCR3/CD183 was determined on lung tissues from **Group 2** patients (**Figure 3**). Numerous CD26+ cells were found in the alveolar septa (**Figure 3, A1-A3**) with intense staining seen in the type II pneumocytes (**Figure 3,A3**). Positive cells entrapped with fibrin clots in the vascular lumen were also observed (**Figure 3,A4**). CXCR3 immunostaining showed lymphocytes localized in inflammatory perivascular aggregates (**Figure 3,B1,B2,B4**) which spread into alveolar septa and alveolar spaces (**Figure 3, B2,B3**).

*Electron microscopic findings:*

SARS-CoV-2 particles were detected within type II pneumocytes which showed degenerating features characterized by fine and uniformly dispersed chromatin. These pneumocytes displayed swollen mitochondrial profiles and dilated rough endoplasmic reticulum (**Figure 4**). Numerous virus containing compartments (VCC) of different size and shape were detected (**Figure 4, A-B,D**). Interestingly, “spherules”, very small vesicles containing single viral particles, (**Figure 4,B,C**) were also observed.

## Heart findings

*Macroscopic findings:*

The hearts in all **Group 1** and **2** patients showed increased in size and weight, hypertrophy and dilation of the left and right atria and ventricles. The myocardium appeared pale and flabby, and endocardium showed punctuate petechial hemorrhages (**Figure 5, A1**). Some patients in **Group 1**, had pathological changes which were related to patient's age. These included myocardial ischemic changes by ischemic or inflammatory changes, hypertensive changes of the left ventricular cavity and valvular calcification of the mitral annulus and aortic valve (**Figure 5,A2**).

*Microscopic findings:*

Microscopic changes seen were: hypertrophy of myocytes, and variable degrees of interstitial and vascular fibrosis (**Figure 5,A3,A4**). Mononuclear cells infiltrating adventitia was found predominantly in **Group 2** patients (**Figure 5, A4**). Active myocarditis (**Figure 5,B1**) characterized by mononuclear, predominantly lymphocytic infiltrate, associated with focal myocytes necrosis

(Figure 5,B2), fibrinous and hemorrhagic areas with myofibers disarray (Figure 5,B3). Pericarditis (fibrinous or fibrous) was mainly seen in **Group 2** patients (Figure 5,B4).

#### **Liver, Kidney, Spleen and Bone Marrow findings**

**Livers:** Macroscopic inspection of the liver of all patients showed parenchyma congestion. Main findings at histological level were sinusoidal congestion and extravasation of red blood cells into the Disse's space (Figure 6,A1); and in a few cases this was associated with congestion of small veins and hepatocyte necrosis (Figure 6,A2,A3) and infiltration (Figure 6,A4). Macrovacuolar and microvacuolar steatosis was seen mostly in Group 2 patients (Figure 6,A1,A2,A4) (Table 3).

**Kidneys:** The kidneys of all patients generally had normal shape with reduced volume and size. Outer surfaces showed reddish depressions. Histological examination showed interstitial fibrosis, mainly in **Group 2** patients (Figure 6,B1), with swollen glomerular endothelial cells. Fibrin deposits were visible underneath the Bowman's capsule (Figure 6,B2). Chronic tubular-interstitial inflammation (Figure 6,B3) and glomerular sclerosis were observed (Figure 6,B4) even in patients without history of previous kidney disease (Table 3).

#### *Spleens:*

The spleens of all patients had normal shape but reduced volume and size. The splenic white pulps of all four of the **Group 2** cases showed lymphoid hypoplasia, with congested red pulp (Figure 7,A1,A2) (Table 3).

#### *Bone marrows:*

Microscopic analysis of the bone marrows generally showed replacement of red hematopoietic bone marrow with yellow adipocyte-rich marrow in **Group 1** patients (Figure 7, B1). Megakaryocytes hyperplasia (Figure 7,B2) was seen in two patients of **Group 2** (Table 3). Numerous macrophages (CD68+) were seen and they displayed features of haemophagocytosis (Figure 7,C1,C2).

## **DISCUSSION**

Whole-body autopsies offer several advantages over limited sampling using biopsies and tissues obtained post-mortem [4-7]. Full body autopsy studies of COVID-19 patients have been scanty due to several issues of infection control and logistical and operational reasons. Whole body autopsy allows examination of most body organs, define extent COVID-19 pathology and also

allows adequate tissue to be obtained for further pathological and molecular evaluation and for research purposes. They also allow a more accurate diagnosis to be made and minimize the chances of missing an accurate diagnosis due to sampling error. Supporting the call for action to conduct full autopsies on patients who die of COVID-19 for determining the extent of organ involvement [12,13], we conducted a comprehensive post-mortem full autopsy examination of twenty-two patients. To our knowledge, our study is the first to report pathological features of 4 cases of COVID-19 who did not have any prior underlying comorbidity or causes of immunosuppression.

Our observations add further information on the pathology examination findings of COVID-19. An initial report from China described histopathologic findings in two cancer patients with COVID-19 showing several nonspecific histologic changes, edema, fibrinous, proteinaceous exudates, hyperplastic pneumocytes, patchy inflammation, and multinucleated giant cells [4]. A case report, also from China, described findings in a postmortem biopsy specimen which showed DAD and interstitial mononuclear inflammatory infiltrates [5]. In our autopsy study, we found that COVID-19 predominantly causes acute lung injury and diffuse alveolar damage, which is associated with multisystem involvement and significant pathology across most body organs in patients with and without co-morbid disease. All deaths were due to cardiorespiratory failure and all cases had extra-pulmonary manifestations. Microvascular injury and thrombosis were also detected. The four younger patients without pre-existing medical conditions also had similar findings despite absence of co-morbidities and displayed all histopathological hallmarks of widespread vascular injury including liver, kidney, spleen and bone marrow involvement.

Our lung pathology findings were similar to those seen in a study of post-mortem lung tissues from northern Italy 33 males and 5 female, patients with an average age of 69 years (range 32-86) [17]. In addition, using electron microscopy we identified viral particles in the cytoplasm of type II pneumocytes - the main target of viral infection [18]. Interestingly, all the histological hallmarks of interstitial pneumonia and capillary damage were prominent in all 22 COVID-19 cases with T lymphocytes being prominent in vascular infiltrates (vasculitis) and interstitial inflammation.

Clinical studies have indicated that Acute Respiratory Distress Syndrome (ARDS) and multiple organ failure are features of severe cases of COVID-19. These are thought to be underpinned by an excessive immune response [19]. In the lung microenvironment, excessive inflammatory cytokine may be caused by immune-pathological changes, linked to lymphocytic infiltration. We

demonstrated a significant upregulation of the chemokine receptor CXCR3, which is not only responsible for T cells extravasating from blood vessels and migration [20], but it has been also implicated in pulmonary fibrosis [21]. It is thus possible that this could be associated with an aberrant type I immune response involving the CXCR3/ligand pathway. In addition, we also found intense expression of CD26/DPP4 (dipeptidyl peptidase-4), a protein that plays a key role for T cell signal transduction processes as a costimulatory molecule, and its expression level is known to correlate with the severity of inflammation [22]. Thus, the CXCR3 cytokine axis could be considered a potential therapeutic target in development of targeted host-directed therapies for COVID-19.

Several publications have shown an association of the severity of the clinical expression of COVID-19 with the number of co-morbidities present. Cardiac involvement in severe COVID-19 pathogenesis has been well documented [23], and cardiac risk factors have been identified as risk factors for increased mortality [24]. In our study of the macroscopic and microscopic features of hearts we found several differences between patients with and without co-morbidities. Those four cases without co-morbidities showed pronounced pericarditis and inflammatory cells infiltrating adventitia, indicating that the heart can be compromised irrespective of previous cardiovascular disease. Kidney injury has been reported in nearly 30% of COVID-19 patients [25]. We found that histopathological changes in kidney in patients without co-morbidities appeared more severe than those without. Patients without co-morbidities also showed greater hepatic injury. Whether these findings represent liver or kidney damage caused directly by SARS-CoV-2 itself or they reflect the consequences of an abnormal and excessive inflammatory response, requires to be defined [26]. Studies of other viral infections of the respiratory tract have shown that liver injury may be immune mediated or a result of direct cytopathic damage [27].

Our study showed that the spleen and bone marrow were affected in 2 of 4 of our patients without co-morbidities. Microscopic analyses of bone marrow showed white pulp lymphoid hypoplasia and megakaryocytes hyperplasia. These hematopoietic organs could be reservoirs of SARS-CoV infection [28] and may directly infect hematopoietic stem/progenitor cells, megakaryocytes and platelets [29]. Microvascular damage and thrombosis were also more pronounced even in cases without pre-existing comorbidities. This supports the known observation that anticoagulant treatment can reduce mortality in COVID-19 [30]. Patients with

COVID19 without any co-morbidities appear to have similar pathological manifestations as those with co-morbidities [31].

There were several limitations of our generic to that of all autopsy studies. Whilst the COVID-19 cases in our study were from across a range of ages, gender, co-morbidities, in lieu of the large number of deaths reported from Italy, we cannot accurately say our findings are fully representative of COVID-19 pathology in the large numbers who died. A range of neurological manifestations of COVID-19 have been reported [35]. We were unable to obtain brain tissue in our study due to infection control regulations. A recent study [36] performed histopathological examination of brain specimens obtained from COVID-19 patients who died up to 32 days after symptom onset, found only hypoxic changes and no specific brain changes attributable to SARS-CoV-2. Further pathological examination of brain tissues need to be performed where cytoplasmic viral staining, immunohistochemical and EM analysis may shed further light on the neuropathological manifestations of COVID-19. It is important that autopsy studies are given priority. Whole-body complete autopsy studies from across a wide range of geographical backgrounds, age, ethnic groups, co-morbidities [32-34] are required to define the pathogenesis and the whole spectrum of pathology of COVID-19.

### Acknowledgments

The authors gratefully acknowledge the excellent support of a) the INMI pathology team: Alessia Brenna, Marco Canali, Roberta Chiappini, Mario Moauro, Nicolina Rotiroti, Wilfredo von Lorch, who risked SARS-CoV-2 infection in performing the autopsies and collecting the samples, b) Professor Sebastian Lucas, emeritus Professor at St Thomas Hospital, London, United Kingdom.

This work was supported in part by grants from the Ricerca Corrente (linea 1and 3) e Finalizzata from the Ministry of Health, AIRC (IG2018-21880 to M.P.), Regione Lazio (Gruppi di ricerca, E56C18000460002, to M.P.). M.P. also acknowledges the support of the grant from the Russian Government Program for the Recruitment of the Leading Scientists into the Russian Institutions of Higher Education (14.W03.31.0029 to M.P.).

Professor Ippolito and Sir Zumla are co-PIs of the Pan-African Network on Emerging and Re-Emerging Infections (PANDORA-ID-NET – <https://www.pandora-id.net/>) funded by the European and Developing Countries Clinical Trials Partnership the EU Horizon 2020 Framework Programme for Research and Innovation. Sir Zumla is in receipt of a National Institutes of Health Research

senior investigator award and is a Mahathir Foundation Science Award Laurette. Professor Ippolito and Dr Vairo are supported by the Italian Ministry of Health (Ricerca Corrente Linea 1). Roberta Nardacci and Delia Goletti are Professors at Saint Camillus International University of Health and Medical Sciences in Rome.

We gratefully acknowledge the assistance of Collaborators Members of INMI COVID-19 study group: Maria Alessandra Abbonizio, Amina Abdeddaim, Chiara Agrati, Fabrizio Albarello, Gioia Amadei, Alessandra Amendola, Mario Antonini, Andrea Antinori, Tommaso Ascoli Bartoli, Francesco Baldini, Raffaella Barbaro, Bardhi Dorian, Barbara Bartolini, Rita Bellagamba, Martina Benigni, Nazario Bevilacqua, Gianlugi Biava, Michele Bibas, Licia Bordi, Veronica Bordoni, Evangelo Boumis, Marta Branca, Donatella Busso, Marta Camici, Paolo Campioni, Maria Rosaria Capobianchi, Alessandro Capone, Cinzia Caporale, Emanuela Caraffa, Ilaria Caravella, Fabrizio Carletti, Concetta Castilletti, Adriana Cataldo, Stefano Cerilli, Carlotta Cerva, Roberta Chiappini, Pierangelo Chinello, Carmine Ciaralli, Stefania Cicalini, Francesca Colavita, Daniele Colombo, Angela Corpoltengo, Massimo Cristofaro, Salvatore Curiale, Alessandra D'Abramo, Cristina Dantimi, Alessia De Angelis, Giada De Angelis, Franca Del Nonno, Maria Grazia De Palo, Federico De Zottis, Virginia Di Bari, Rachele Di Lorenzo, Federica Di Stefano, Gianpiero D'Offizi, Davide Donno, Laura Falasca, Francesca Faraglia, Federica Ferraro, Lorena Fiorentini, Andrea Frustaci, Matteo Fusetti, Vincenzo Galati, Roberta Gagliardini, Paola Galli, Gabriele Garotto, Saba Gebremeskel Tekle, Maria Letizia Giancola, Filippo Giansante, Emanuela Giombini, Guido Granata, Maria Cristina Greci, Elisabetta Grilli, Susanna Grisetti, Gina Gualano, Fabio Iacomi, Giuseppina Iannicelli, Giuseppe Ippolito, Eleonora Lalle, Simone Lanini, Daniele Lapa, Luciana Lepore, Raffaella Libertone, Raffaella Lionetti, Giuseppina Liuzzi, Laura Loiacono, Andrea Lucia, Franco Lufrani, Manuela Macchione, Gaetano Maffongelli, Alessandra Marani, Luisa Marchioni, Raffaella Marconi, Andrea Mariano, Maria Cristina Marini, Micaela Maritti, Alessandra Mastrobattista, Ilaria Mastrorosa, Giulia Matusali, Valentina Mazzotta, Paola Mencarini, Silvia Meschi, Francesco Messina, Annalisa Mondi, Marzia Montalbano, Chiara Montaldo, Silvia Mosti, Silvia Murachelli, Maria Musso, Roberta Nardacci, Emanuele Nicastri, Pasquale Noto, Roberto Noto, Alessandra Oliva, Sandrine Ottou, Claudia Palazzolo, Emanuele Pallini, Fabrizio Palmieri, Carlo Pareo, Virgilio Passeri, Federico Pelliccioni, Antonella Petrecchia, Ada Petrone, Nicola Petrosillo, Elisa Pianura, Carmela Pinnetti, Maria Pisciotta, Silvia Pittalis, Agostina Pontarelli, Costanza Proietti, Vincenzo Puro, Paolo Migliorisi Ramazzini, Alessia Rianda, Gabriele Rinonapoli, Silvia Rosati, Martina Rueca, Alessandra Sacchi, Alessandro Sampaolesi, Francesco Sanasi, Carmen Santagata, Alessandra Scarabello, Silvana Scarcia, Vincenzo Schininà, Paola Scognamiglio, Laura Scorzolini, Giulia Stazi, Fabrizio Taglietti, Chiara Taibi, Roberto Tonnarini, Simone Topino, Francesco Vaia, Francesco Vairo, Maria Beatrice Valli, Alessandra Vergori, Laura Vincenzi, Ubaldo Visco-Comandini, Serena Vita, Pietro Vittozzi, Mauro Zaccarelli, Alimuddin Zumla.

**Funding:** Ricerca Corrente (linea 1and 3) e Finalizzata from the Ministry of Health, AIRC (IG2018-21880).

**Conflict of interest.** All authors report no conflicts of interest. All authors have submitted the ICMJE Form for Disclosure of Potential Conflicts of Interest.

**References:**

1. WHO 2020: Coronavirus disease (COVID-19) situation reports.  
<https://www.who.int/emergencies/diseases/novel-coronavirus-2019/situation-reports-accessed-14th-July-2020>
2. Chen N, Zhou M, Dong X, et al. Epidemiological and clinical characteristics of 99 cases of 2019 novel coronavirus pneumonia in Wuhan, China: a descriptive study. Lancet. **2020**; 395:507-513.
3. Chen G, Wu D, Guo W, et al . Clinical and immunological features of severe and moderate coronavirus disease-2019. J Clin Invest. **2020**; 130:2620-2629.
4. Xu Z, Shi L, Wang Y, et al. Pathological findings of COVID-19 associated with acute respiratory distress syndrome. Lancet Respir Med **2020**; 8: 420–422.
5. Tian, S., Xiong, Y., Liu, H. et al. Pathological study of the 2019 novel coronavirus disease (COVID-19) through postmortem core biopsies. Mod Pathol **2020**; 33:1007-1014.
6. Konopka KE, Wilson A, Myers JL. Postmortem Lung Findings in an Asthmatic with Coronavirus Disease 2019. Chest **2020**; S0012-3692(20)30775-3.
7. Su H, Yang M, Wan C, et al. Renal histopathological analysis of 26 postmortem findings of patients with COVID-19 in China. Kidney Int. **2020**; 98:219-227.
8. Wichmann D, Sperhake JP, Lütgehetmann M, et al. Autopsy Findings and Venous Thromboembolism in Patients With COVID-19: A Prospective Cohort Study. Ann Intern Med. **2020**; M20-2003.
9. Menter T, Haslbauer JD, Nienhold R, et al. Post-mortem examination of COVID19 patients reveals diffuse alveolar damage with severe capillary congestion and variegated findings of lungs and other organs suggesting vascular dysfunction. Histopathology. **2020**; doi: 10.1111/his.14134. Online ahead of print.
10. YajunYuan, Wang N, Ou X. Caution should be exercised for the detection of SARS-CoV-2, especially in the elderly. J Med Virol. 2020 Mar 30. doi: 10.1002/jmv.25796. Online ahead of print. PMID: 32227494.
11. CDC March 2020, Interim Guidance; Hanley B, Lucas SB, Youd E, Swift B, Osborn M. Autopsy in suspected COVID-19 cases. J Clin Pathol. **2020**; 73:239-242.
12. Ledford H. Autopsy slowdown hinders quest to determine how coronavirus kills. [published online ahead of print, 2020 May 7]. Nature. **2020**; doi: 10.1038/d41586-020-01355-z. Online ahead of print

13. Xu X, Barth RF, Buja LM. A Call to Action: The Need for Autopsies to Determine the Full Extent of Organ Involvement Associated With COVID-19 [published online ahead of print, 2020 Apr 10]. *Chest*. **2020**; 158:43-44.
14. Baiocchini A, Del Nonno F, Taibi C, Visco-Comandini U, D'Offizi G, Piacentini M, Falasca L. Liver sinusoidal endothelial cells (LSECs) modifications in patients with chronic hepatitis C. *Sci Rep*. **2019**; 9:8760. Erratum in: *Sci Rep*. 2020; 10:1420.
15. Nardacci R, Amendola A, Ciccosanti F, Corazzari M, Esposito V, Vlassi C, Taibi C, Fimia GM, Del Nonno F, Ippolito G, D'Offizi G, Piacentini M. Autophagy plays an important role in the containment of HIV-1 in nonprogressor-infected patients. *Autophagy*. **2014**; 10:1167-78.
16. Klemann C, Wagner L, Stephan M, von Hörsten S. Cut to the chase: a review of CD26/dipeptidyl peptidase-4's (DPP4) entanglement in the immune system. *Clin Exp Immunol*. **2016**; 185:1-21.
17. Carsana L, Sonzogni A, Nasr, A et al. Pulmonary post-mortem findings in a series of COVID-19 cases from northern Italy: a two-centre descriptive study. *Lancet Infect Dis*. 2020 Jun 8:S1473-3099(20)30434-5
18. Roberta Nardacci, Francesca Colavita, Concetta Castilletti et al. SARS-CoV-2 cytopathogenesis in cultured cells and in COVID-19 autoptic lung, evidences of lipid involvement., 07 July 2020, PREPRINT (Version 1) available at Research Square [+<https://doi.org/10.21203/rs.3.rs-39274/v1+>]
19. Ye Q, Wang B, Mao J. The pathogenesis and treatment of the 'Cytokine Storm' in COVID-19. *J Infect*. **2020**; 80: 607-613.
20. Moser B, Wolf M, Walz A, Loetscher P. Chemokines: multiple levels of leukocyte migration control. *Trends Immunol* **2004**; 25:75–84.
21. Jiang D, Liang J, Hodge J, Lu B, Zhu Z, Yu S, Fan J, Gao Y, Yin Z, Homer R, Gerard C, Noble PW. Regulation of pulmonary fibrosis by chemokine receptor CXCR3. *The Journal of Clinical Investigation* **2004**; 114: 291–9.
22. Kruschinski C, Skripuletz T, Bedoui S, et al. CD26 (dipeptidyl-peptidase IV)-dependent recruitment of T cells in a rat asthma model. *Clin Exp Immunol*. **2005**; 139:17-24.
23. Zhang H, Penninger JM, Li Y, Zhong N, Slutsky AS. Angiotensin-converting enzyme 2 (ACE2) as a SARS-CoV-2 receptor: molecular mechanisms and potential therapeutic target. *Intensive Care Med*. **2020**; 46:586-590.
24. Aghagoli G, Gallo Marin B, Soliman LB, Sellke FW. Cardiac involvement in COVID-19 patients: Risk factors, predictors, and complications: A review. *J Card Surg*. **2020**; 35:1302-1305.
25. Diao B, Feng Z, Wang C, Wang H, Liu L, Wang C, et al. Human kidney is a target for novel severe acute respiratory syndrome coronavirus 2 (SARS-CoV-2) infection. *medRxiv*. **2020**; 2020.03.04.20031120. Available from: <https://doi.org/10.1101/2020.03.04.20031120>

26. Xu L, Liu J, Lu M, Yang D and Zheng X. Liver injury during highly pathogenic human coronavirus infections. *Liver Int.* **2020**; 40:998-1004.
27. Feng G, Zheng KI, Yan QQ, Rios RS, Targher G, Byrne CD, Poucke SV, Liu WY, Zheng MH. COVID-19 and Liver Dysfunction: Current Insights and Emergent Therapeutic Strategies. *J Clin Transl Hepatol.* **2020**; 8:18-24.
28. Gu J, et al. Multiple organ infection and the pathogenesis of SARS. *J Exp Med.* **2005**; 202:415-24.
29. Yang M, Ng MH, Li CK. Thrombocytopenia in patients with severe acute respiratory syndrome (review). *Hematology.* **2005**; 10:101-5.
30. Tang N, Bai H, Chen X, Gong J, Li D, Sun Z. Anticoagulant treatment is associated with decreased mortality in severe coronavirus disease 2019 patients with coagulopathy. *J Thromb Haemost.* **2020**; 18:1094-1099.
31. Hui Li, Liang Liu, Dingyu Zhang, Jiuyang Xu, Huaping Dai, Nan Tang, Xiao Su, Bin Cao. SARS-CoV-2 and Viral Sepsis: Observations and Hypotheses. *Lancet.* **2020**; 395:1517-1520.
32. Yajun Yuan, Wang N, Ou X. Caution should be exercised for the detection of SARS-CoV-2, especially in the elderly. *J Med Virol.* **2020** Mar 30. doi: 10.1002/jmv.25796. Online ahead of print.
33. Guan WJ, Liang WH, Zhao Y, Liang HR, Chen ZS, Li YM, Liu XQ, et al. Comorbidity and its impact on 1590 patients with Covid-19 in China: A Nationwide Analysis. *Eur Respir J.* **2020**; 55:2000547.
34. Richardson S, Hirsch JS, Narasimhan M, et al. Presenting Characteristics, Comorbidities, and Outcomes Among 5700 Patients Hospitalized With COVID-19 in the New York City Area. *JAMA.* **2020**; 323:2052-2059.
35. Solomon IH, Normandin E, Bhattacharyya S, et al. Neuropathological Features of Covid-19. *N Engl J Med.* **2020**; NEJMc2019373. Online ahead of print.
36. Nepal G, Rehrig JH, Shrestha GS, et al. Neurological manifestations of COVID-19: a systematic review. *Crit Care.* **2020**; 24:421.

**Table 1**  
**Summary - Patients' demographics at baseline**

|  | <b>Group 1<br/>(With co-morbidities)</b> | <b>Group 2<br/>(No co-morbidities)</b> |
|--|--|--|
| <b>Number of Patients</b>                    | <b>18</b>                                | <b>4</b>                               |
| <b>Demography</b>                            |  |  |
| <b>Age* (years)</b>                          | $76 \pm 15.7$ ( 27-92)                   | $48.5 \pm 13.07$ (35-65)               |
| <b>Men (%)</b>                               | 12 (66.7%)                               | 3 (75%)                                |
| <b>Women (%)</b>                             | 6 (33.3%)                                | 1 (25%)                                |
|  |  |  |
| <b>Chronic Obstructive Pulmonary disease</b> | 6 (33.3%)                                |  |
| <b>Cardiac disease</b>                       | 8 (44.5%)                                |  |
| <b>Malignancy</b>                            | 5 (27.8%)                                |  |
| <b>Hypertension</b>                          | 4 (22.3%)                                |  |
| <b>Diabetes</b>                              | 4 (22.3%)                                |  |
| <b>Schizophrenia</b>                         | 1 (5.6%)                                 |  |
| <b>Kidney disease</b>                        | 2(11.2%)                                 |  |

\* Median  $\pm$  SD; years (range)

**Table 2**
**Demographics, Co-morbidities, Duration of hospital stay and Autopsy cause of death**

| Patient Number | Gender (M/F) | Age (yrs) | Onset of symptoms (duration, days) | Co-morbidities   | Days in hospital before death | Post-mortem cause of death |
|----------------|--------------|-----------|------------------------------------|--|-------------------------------|----------------------------|
| 1              | M            | 81        | Not known                          | Hypertension<br>Aorto-myocardial sclerosis<br>Ischemic heart disease<br>Cardiomyopathy<br>Aortic aneurysm  | 4                             | Cardiorespiratory failure  |
| 2              | F            | 82        | Not known                          | Diabetes<br>Atrioventricular valve prosthesis<br>Atrial fibrillation<br>Chronic obstructive pulmonary disease (COPD)<br>Malignancy<br>Kidney disease | 3                             | Cardiorespiratory failure  |
| 3              | M            | 92        | 7                                  | COPD   | 1                             | Cardiorespiratory failure  |
| 4              | F            | 69        | Not known                          | Schizophrenia  | 28                            | Cardiorespiratory failure  |
| 5              | F            | 80        | Not known                          | Cardiovascular disease<br>Senile dementia  | 38                            | Cardiorespiratory failure  |
| 6              | M            | 92        | Not known                          | Cardiovascular disease<br>COPD   | 3                             | Cardiorespiratory failure  |
| 7              | F            | 64        | 4                                  | Malignancy   | 2                             | Cardiorespiratory failure  |
| 8              | M            | 58        | Not known                          | Pulmonary artery thrombosis  | 4                             | Cardiorespiratory failure  |
| 9              | M            | 64        | Not known                          | Myelodysplasia   | 4                             | Cardiorespiratory failure  |
| 10             | M            | 82        | 3                                  | Aortic aneurysm<br>COPD  | 5                             | Cardiorespiratory failure  |
| 11             | M            | 76        | Not known                          | Malignancy   | 30                            | Cardiorespiratory failure  |
| 12             | M            | 60        | 6                                  | Malignancy   | 29                            | Cardiorespiratory          |

|           |   |    |           |   |    |                           |
|-----------|---|----|-----------|---|----|---------------------------|
|           |   |    |           | Hypertension<br>Kidney disease<br>Diabetes<br>COPD<br>Obesity   |    | failure                   |
| <b>13</b> | F | 70 | Not known | Cardiovascular disease<br>Diabetes<br>Psychiatric disorder  | 43 | Cardiorespiratory failure |
| <b>14</b> | M | 76 | Not known | Malignancy<br>COPD<br>Hypertension<br>Cardiovascular disease  | 33 | Cardiorespiratory failure |
| <b>15</b> | F | 27 | Not known | HIV infection   | 6  | Cardiorespiratory failure |
| <b>16</b> | M | 82 | Not known | Parkinson's disease<br>Hypertension<br>Transient ischemic attack (TIA)<br>Prostate hypertrophy                        | 14 | Cardiorespiratory failure |
| <b>17</b> | M | 57 | Not known | Diabetes  | 1  | Cardiorespiratory failure |
| <b>18</b> | M | 86 | Not known | Endocarditis caused by <i>Staphylococcus aureus</i><br>Prostate hypertrophy<br>Aortic aneurysm<br>Atrial fibrillation | 1  | Cardiorespiratory failure |
| <b>19</b> | M | 54 | 4         | NONE  | 16 | Cardiorespiratory failure |
| <b>20</b> | M | 35 | 5         | NONE  | 7  | Cardiorespiratory failure |
| <b>21</b> | M | 65 | 7         | NONE  | 12 | Cardiorespiratory failure |
| <b>22</b> | F | 43 | Not known | NONE  | 25 | Cardiorespiratory failure |

**Table 3**  
**Histopathology findings**

|   | <b>Group 1<br/>n=18</b> | <b>Group 2<br/>n=4</b> |
|---|-------------------------|------------------------|
| <b>Lung findings</b>                                    |                         |                        |
| Diffuse alveolar damage (exudative/proliferative phase) |                         |                        |
| Hyaline membranes                                       | 8 (44.4%)               | 2 (50%)                |
| Hyperplasia of type II pneumocyte                       | 11 (61.2%)              | 4 (100%)               |
| Alveolar plug   | 8 (44.4%)               | 4 (100%)               |
| Alveolar fibrin deposit                                 | 9 (50%)                 | 3 (75%)                |
| Hemorrhage  | 10 (55.6%)              | 2 (50%)                |
| Inflammatory cells                                      | 13 (72.3%)              | 4 (100%)               |
| Diffuse alveolar damage (fibrotic phase)                | 12 (66.7%)              | 1 (25%)                |
| Microthrombi  | 14 (77.8%)              | 2 (50%)                |
| Vasculitis  | 8 (44.4%)               | 4 (100%)               |
| Multinucleated giant cells                              | 4 (22.3%)               | 2 (50%)                |
| <b>Cardiac findings</b>                                 |                         |                        |
| Myocarditis   | 9 (50%)                 | 3 (75%)                |
| Vasculitis  | 5 (27.8%)               | 3 (75%)                |
| Inflammatory infiltrate                                 | 13 (72.3%)              | 3 (75%)                |
| Focal necrosis  | 6 (33.4%)               | 2 (50%)                |
| Pericarditis  | 9 (50%)                 | 4 (100%)               |
| Vascular fibrosis                                       | 4 (22.3%)               | 2 (50%)                |
| <b>Hepatic findings</b>                                 |                         |                        |
| Inflammatory infiltrate                                 | 8 (44.4%)               | 3 (75%)                |
| Congestion  | 8 (44.4%)               | 2 (50%)                |
| Steatosis   | 9 (50%)                 | 3 (75%)                |
| <b>Renal Findings</b>                                   |                         |                        |
| Inflammatory infiltrate                                 | 9 (50%)                 | 3 (75%)                |
| Glomerulosclerosis                                      | 9 (50%)                 | 3 (75%)                |
| Interstitial fibrosis                                   | 9 (50%)                 | 4 (100%)               |
| <b>Splenic findings</b>                                 |                         |                        |
| Congested red pulp                                      | 15 (83.4%)              | 4 (100%)               |
| Lymphoid hypoplasia                                     | 11 (61.2%)              | 4 (100%)               |
| <b>Bone marrow findings</b>                             |                         |                        |
| Megakaryocytes hyperplasia                              | 0%                      | 2 (50%)                |
| Adipocytes  | 7 (38.9%)               | 1 (25%)                |

## Figures

**Figure 1. Pathological findings in lung.** (A1) Lungs show increase in volume, and were firmer and heavier than normal. (A2,A3) Light microscopic analysis shows parenchymal multifocal damage with intra-alveolar inflammation, fibrin, hyaline membranes consistent with a diagnosis of diffuse alveolar damage. Both acute exudative inflammatory process and fibrous proliferative phase are found. (A3,A4) Hyperplasia of type II pneumocyte, characterized by amphophilic cytoplasm, large nuclei and prominent nucleoli are shown (arrows). (B1) Alveolar duct fibrosis. (B2) Fibrin thrombi found in capillaries. (B3) Vascular injury including vessel vasculitis and vascular edema. (B4) Pleural fibrosis.

Scale bars: B = 14  $\mu\text{m}$ ; C-G = 7 $\mu\text{m}$ ; H = 21 mm

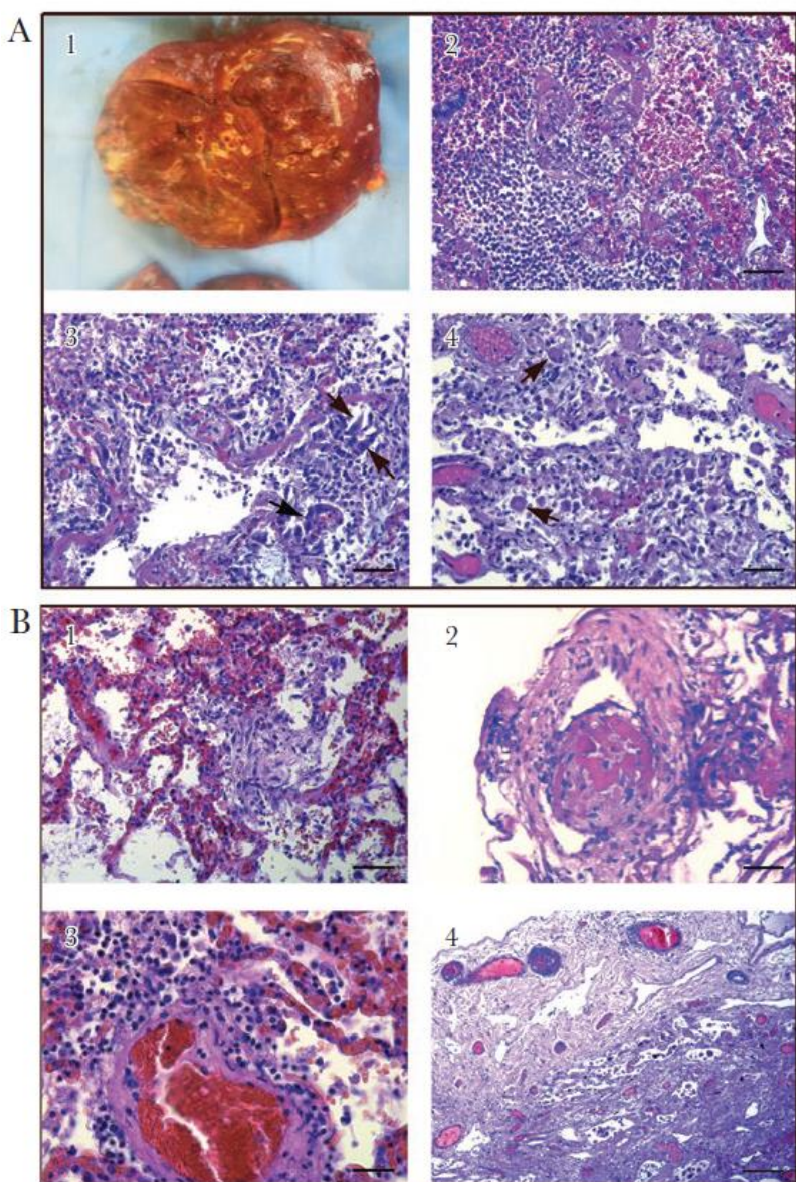


**Figure 2. Immunohistology of lung tissue.**

Immunohistological characterization of lung tissue.

(A1-A4) CD26/DPP4 expression in lung tissue. Numerous strongly positive CD26+ cells are seen in the alveolar septa. (A3) Intense staining is seen in the type II pneumocytes (arrows). (A4) Positive cells are also seen entrapped with fibrin in the vascular lumen. (B1-B4) CXCR3/CD183 immunostaining shows intense staining of lymphocytes localized in the inflammatory perivascular aggregates and spread into alveolar septa and alveolar spaces.

Scale bars: A,E = 100  $\mu$ m; B, C,H = 7  $\mu$ m; D,F,G = 14  $\mu$ m.

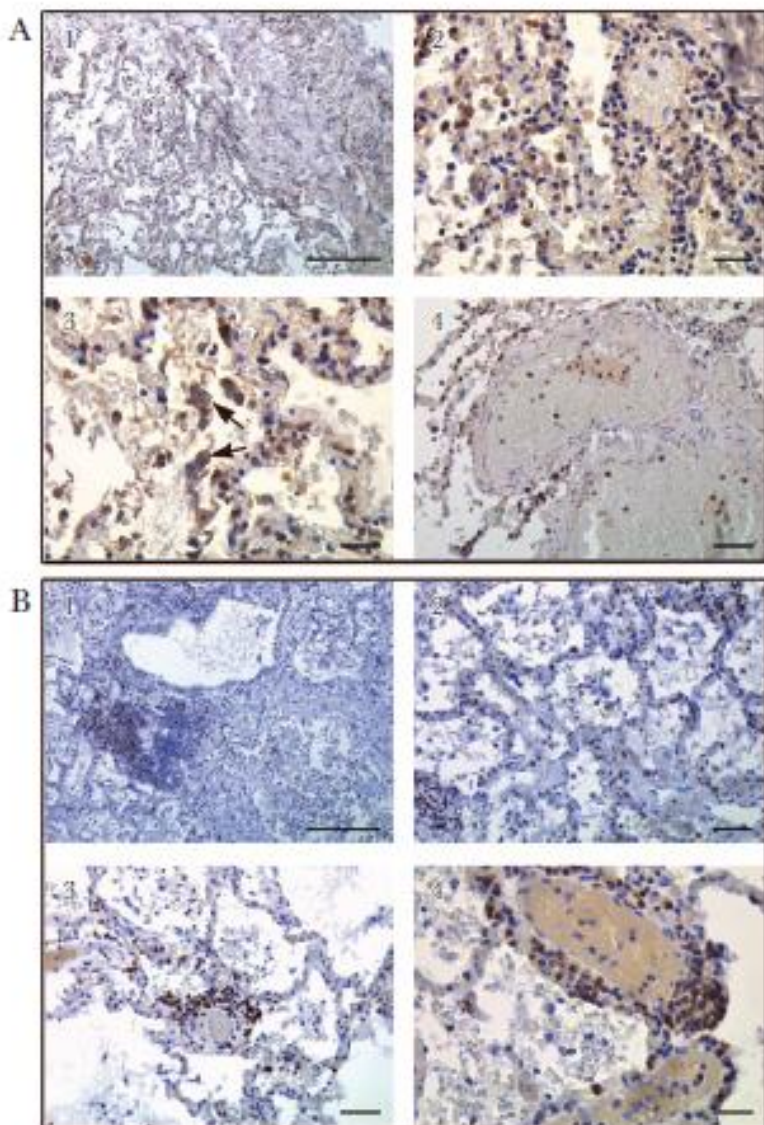


**Figure 3.**

SARS-CoV-2 detection in lung tissue by transmission electron microscopy.

(A) SARS-CoV-2 particles are visible in virus containing compartments in type II pneumocytes (arrows). (B-D) Numerous viral particles are enclosed in single membrane vacuole (arrow). Other vesicles, very small in size, contain single viral particles (arrowheads).

Scale bars: A = 1 $\mu$ m; B-D = 200nm

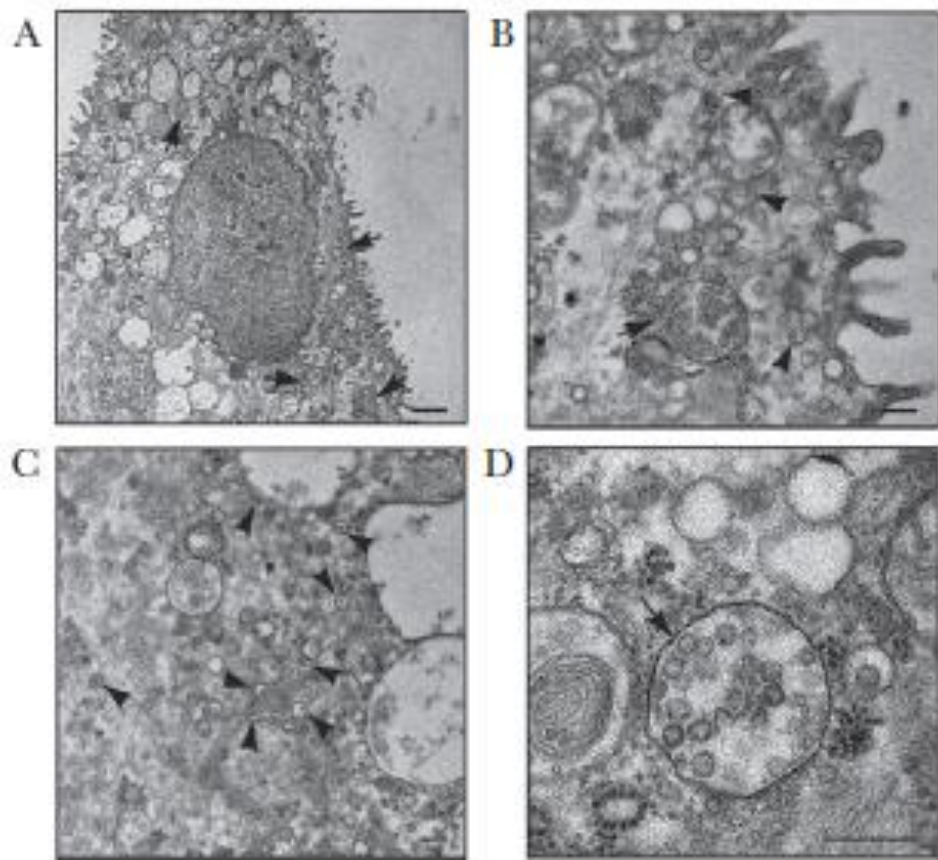


**Figure 4. Histological changes in heart.**

(A1) The heart is increased in the size and in weight. The myocardium appeared pale and flabby. Endocardium shows punctuate petechial hemorrhages. (A2) Age related disease of the heart is represented by volume changes of the left ventricular cavity and is exacerbated by systemic hypertension with valve changes including calcification of the mitral annulus and aortic valve. (A3,A4) heart tissue show myocytes hypertrophy, variable degrees of interstitial and vascular fibrosis with mononuclear cells infiltrating adventitia. (B1) Active myocarditis is characterized by mononuclear, predominantly lymphocytic infiltrate, associated with focal myocytes necrosis (B2). (B3) Fibrinous, hemorrhagic areas with myofibers disarray are present. (B4) Pericarditis with lymphocytic infiltration and increase in fibrous tissue is seen in all patients.

Scale bars: C,H = 21  $\mu$ m; D-F= 7 $\mu$ m; G = 14 $\mu$ m.

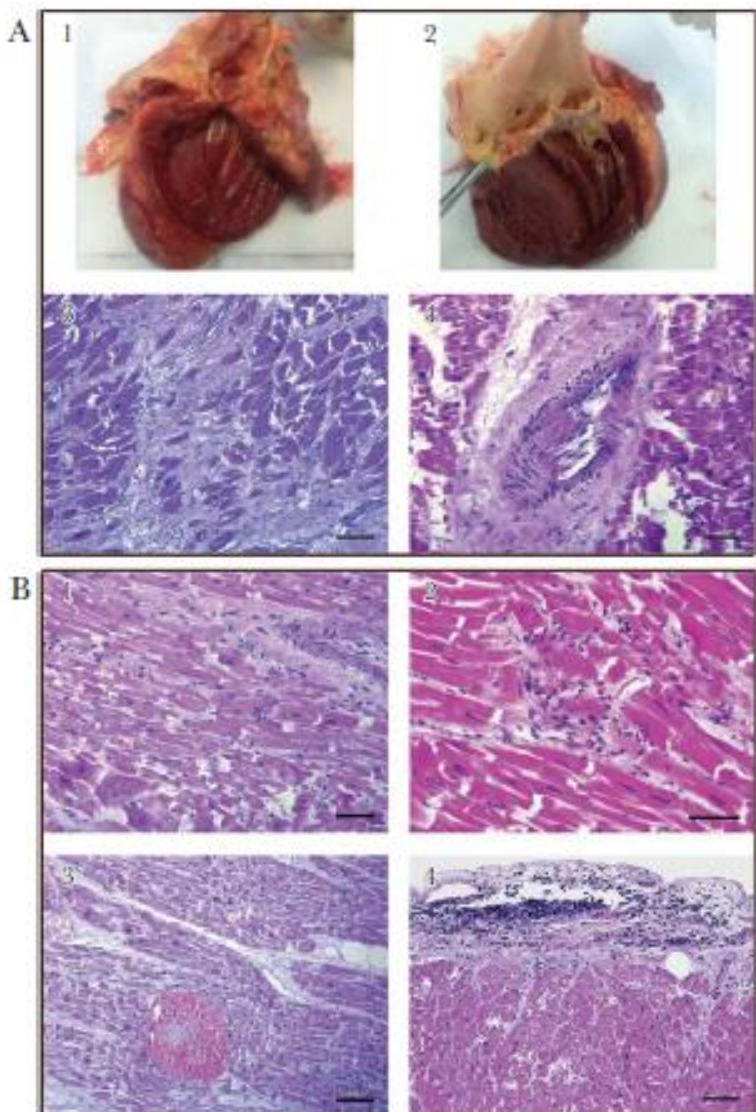


**Figure 5.**

Pathological findings in liver and kidney. (A1) Liver tissue shows sinusoidal congestion and extravasation of red blood cells into the space of Disse. In some cases is reported (A2) small veins congestion and (A3) hepatic necrosis. (A4) Inflammatory infiltration is observed. (A1,A2,A4) Macrovacuolar and microvacuolar steatosis is observed in the majority of cases. (B1) Kidney glomerular endothelial cells are swollen. (B2) Fibrin deposit is visible underneath the Bowman's capsule. (B3) Tubulointerstitial inflammation and (B4) glomerular sclerosis are observed.

Scale bars: A-D,G=50  $\mu$ m; E,F,H = 14  $\mu$ m

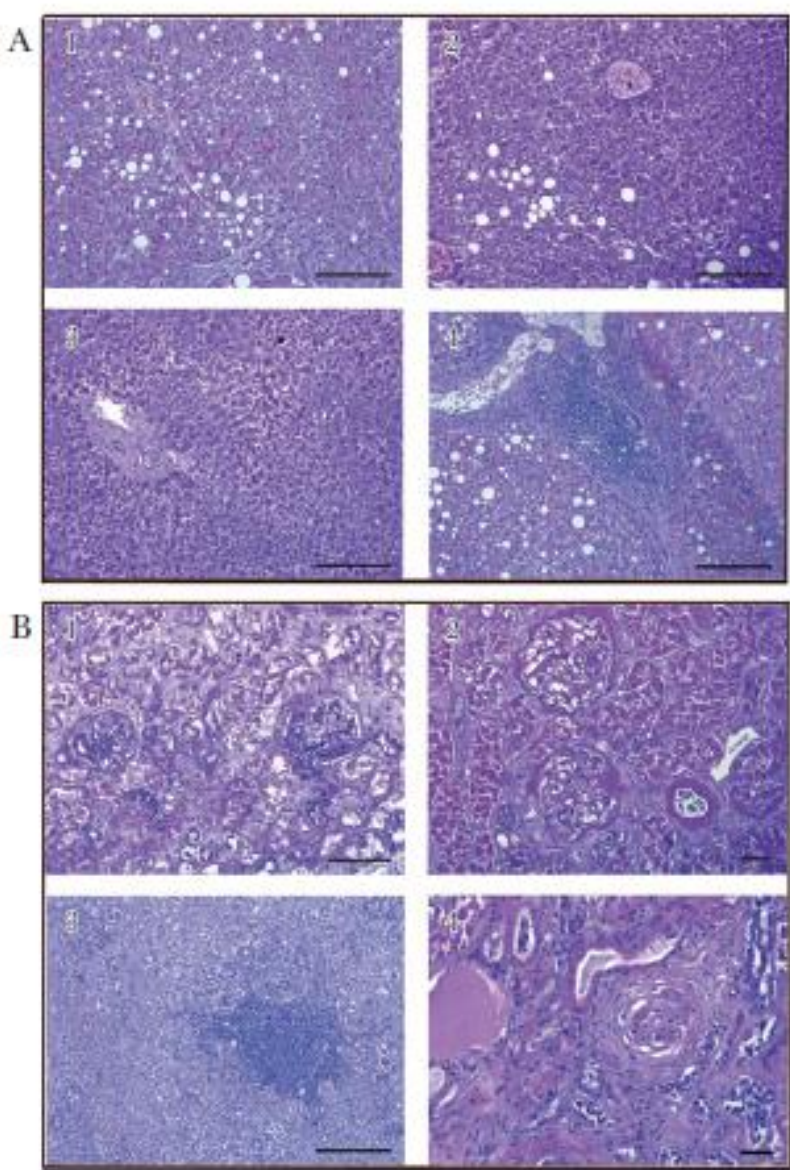


**Figure 6. Histology of spleen and bone marrow.**

(A1,A2). Lymphoid hypoplasia is visible in the splenic white pulp. (B1,B2) Bone marrows tissue reveal replacement of red hematopoietic bone marrow with yellow adipocyte-rich marrow. Megacaryocytes hyperplasia is observed (arrows). (C1) Macrophages (CD68+) are present in bone marrow tissue. (C2) CD68+ cell displaying features of haemophagocytosis (arrow).

Scale bars: A,B,D,E,F= 7  $\mu$ m; C = 100  $\mu$ m.

